Proceedings of the
American Control Conference
Baltimore, Maryland • June 1994

DESIGN AND CONSTRUCTION OF A SMALL DUCTED FAN ENGINE FOR NONLINEAR CONTROL EXPERIMENTS

HENRY CHOI, PETER STURDZA, AND RICHARD M. MURRAY

Department of Mechanical Engineering
California Institute of Technology
Pasadena, California 91125

Abstract

This paper describes the design and construction of a small ducted fan engine which is being used for experimental research in robust nonlinear control of high-performance vectored thrust aircraft. The fan consists of a high-efficiency electric motor with a 6-inch diameter blade, capable of generating up to 9 Newtons of thrust. Flaps on the fan allow the thrust to be vectored from side to side and even reversed. The engine is mounted on a three degree of freedom stand which allows horizontal and vertical translation as well as unrestricted pitch angle. We give a detailed description of the design and construction of the fan and its analytical and empirical models. Initial PID controllers for altitude and pitch angle stabilization are included to verify the system model and indicate future avenues of research.

1. Introduction

We have recently undertaken a study of the problem of robust control of nonlinear systems, directed towards applications in control of high-performance jet aircraft. Very few design methods are currently available for building robust, nonlinear control laws for this class of systems. We are concentrating on the control of an aircraft powered by a ducted fan engine, transitioning between hover and forward flight. By focusing on a specific nonlinear system, we hope to generate new ideas and techniques for applying the tools of robust linear control theory to systems with strongly nonlinear behavior.

In this paper we describe the design and construction of a small ducted-fan engine which shares many of the basic characteristics of more complicated flight control systems. A picture of the fan unit is shown in Figure 1.

There is a large literature on vectored propulsion systems and they are gaining in popularity as a method of improving the performance capabilities of modern jet aircraft. The fundamental concepts in vectored propulsion are described by Gal-Or [1]. Most of the existing literature and experiments concentrate on control of full-scale jet engines and are primarily concerned with extending the flight envelope by extending existing (linear) control methodologies. Our goal is to build a test station in which we can explore the nonlinear nature of flight control systems in a laboratory setting. We are currently aware of only one other experiment which is similar to ours, being built by J. Hauser at the University of Colorado, Boulder.

2. Experimental Setup

The overall experimental setup consists of a ducted fan attached to a three degree of freedom stand, as shown in Figure 2. The main design philosophy was to have a relatively simple ducted fan aircraft which could provide two dimensional vectored and reverse thrust. The aircraft

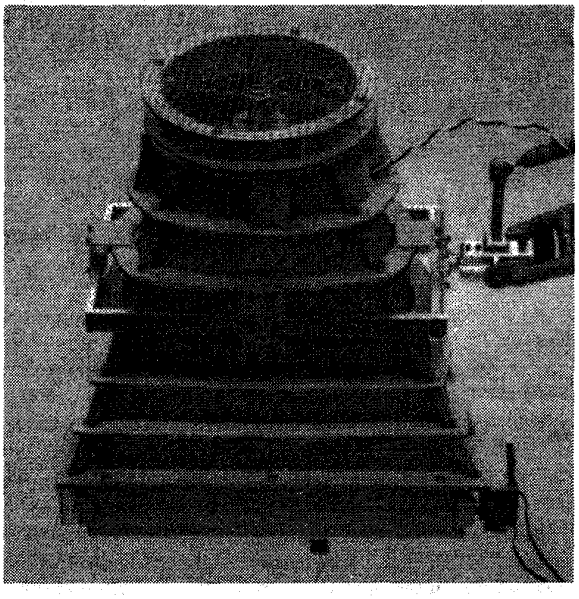

Figure 1: Ducted fan apparatus

is bolted to a rotating arm so as to limit it to three degrees of freedom: one rotational and two translational, approximately on the surface of a sphere defined by the arm. With this geometry, the ducted fan is completely controllable with just the vectored thrust.

2.1. Fan construction. The model aviation industry offers accurate actuator servos, speed controllers and electric motors for aircraft of this size. The duct was designed around a high efficiency electric motor driving a pair of six-inch propellers placed ninety degrees apart. Flap unit placed at the aft of the duct provides vectored thrust. In order to accommodate a simple flap assembly, the duct cross-section changes from circular to rectangular shape with a final aspect ratio of about 7:1. The motor can generate approximately 9 Newtons of thrust in still air, with a rotational speed of approximately 10,000 rpm.

McCormick [3] and Kuchemann and Weber [2] show that a properly designed ideal duct can augment the thrust of a propeller. In general, this implies that the duct area should be at a minimum at the propeller, and then increase towards the exit. Since increasing the area in the duct may aggravate the boundary layer effect in the duct, especially with the changing cross-section shape, a constant cross-sectional area duct was chosen.

The duct was designed from a construction viewpoint, not an aerodynamic one. The cross-sections are such that four straight longitudinal load carrying members can be used as the "backbone." The intake and the flap assembly can be easily removed for maintenance

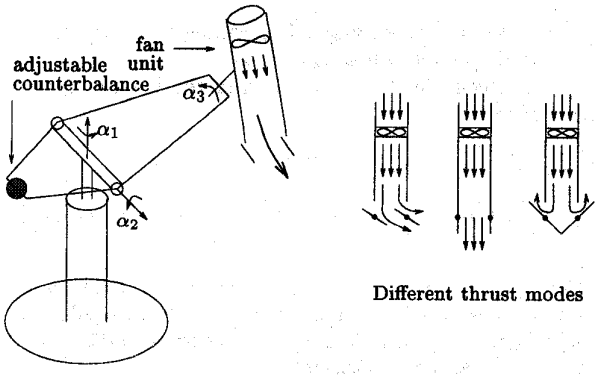

Figure 2: Overview of the experimental apparatus and thrust figures for different flap settings

and improvement. For example, since the intake section–which was added on purely out of safety concerns–is a major source of fan noise, a more aerodynamic intake section is being designed and will replace the current intake. The basic duct itself is 14 inches long. Since the aircraft is currently counterbalanced by the arm, the 9 Newtons of maximum static thrust it delivers is sufficient for control experiments.

The idea for a pair of deflectors placed at the aft of the duct came from the deflector unit on F-15-S/MTD demonstrator [1]. This flap arrangement (see Figure 2) is easy to fabricate and capable of generating vectored and even reverse thrust. Each flap is hinged at the center and connected directly to its own R/C servo with maximum torque of slightly less than 50 oz-in (3.5 kg-cm), so that they can be commanded independently to give vectored and even reverse thrust by closing off the back end, in a similar manner to the clam shell reversers on commercial aircraft.

A rectangular shaped aluminum bracket and four U-shaped aluminum holders connect the wooden construction to α_3 axis shaft, which hangs out at the end of the stand. Three sets of bolt holes were drilled in the bracket, so that the center of mass of the fan could be placed above or below the center or rotation. This allows both stable and unstable plant configurations to be explored.

2.2. Stand construction. The major features of the stand are the counterweight, four bar mechanism, and the slip ring. The counterweight was necessary because the fan, weighing 1.435 kg, was too heavy to lift itself up with the maximum thrust of less than 9 Newtons. Also, by adjusting the position and the mass of the counterweight, it is possible to change some physical parameters that affect the stability and performance directly.

The four bar mechanism is the most unique part of the stand assembly. Figure 4 shows its parallelogram geometry, which allows the fan to rotate about an axis that is always parallel to the ground. Due to difficulty in machining the base, the center of mass of the frame (which is referred to as the "base" in the analytical model derived in Section 3. Consequently, the center of mass of the whole system lies below the α_2 (altitude) axis and gives the system added stability in altitude.

Power and control signals are routed to the fan via a slip ring assembly on the first joint (α_1 axis). The slip ring assembly was necessary since forward flight is one of the objectives of the experiment, which meant the fan has

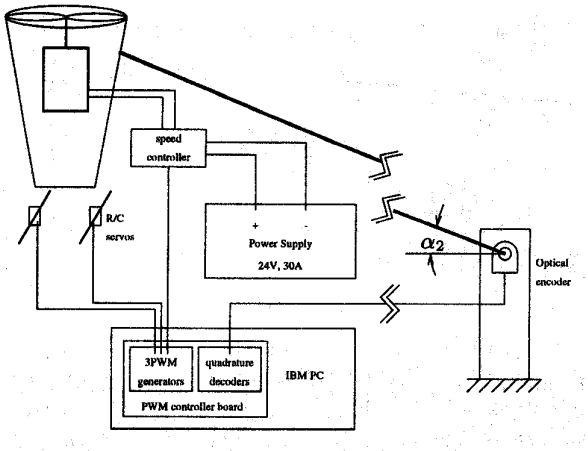

Figure 3: The computer schematic diagram

to be able to go many times around the stand. Although power to the motor is rated at 700 watts at peak, the slip ring could only carry two amperes per channel, with seven channels available for supplying current at 24 volts, delivering 336 watts peak power to the motor. All other signals are carried across the slip ring as well.

2.3. Computer interfacing. The experiment is interfaced to an 80386 computer running an MSDOS-based real-time kernel called Sparrow [4]. This package is a library of C functions that are used in implementation of real-time controllers on a PC-based data acquisition and control system. It contains functions for executing control algorithms at a software selectable rate, communicating with hardware interface cards, displaying, graphing, and capturing data all in real-time. Custom hardware is used to read in joint angles via encoders and generate PWM (pulse width modulation) signals necessary to control the fan motor and the flaps.

Currently, the joint angles are read in at 200Hz and the PWM signals are output at 50Hz, which is the standard update rate for R/C servos. The R/C servos control the flap angles and speed controller controls the motor speed, and consequently the fan force. Figure 3 shows the basic experimental setup. A linear correspondence between the input pulse width and the output angle was experimentally determined and used in the real-time control program to convert the desired flap angles into the PWM pulse width to R/C servos.

An optical encoder with an angular resolution of $\pi \times 10^{-3}$ radians is mounted on each revolute joint of the base. Each encoder signal is decoded with a quadrature decoder, which keeps a running pulse count of the encoder output. The real-time software checks the buffer of the individual decoders to determine the angle that the encoder has turned with respect to its initial position. The configuration of the fan is completely determined from the three joint angles.

3. System identification

3.1. Model derivation. The equations of the motion for the system can be easily derived using Lagrange's equation from the simplied version of the picture of the overall experimental setup, as shown in Figure 4. We use the following notation:

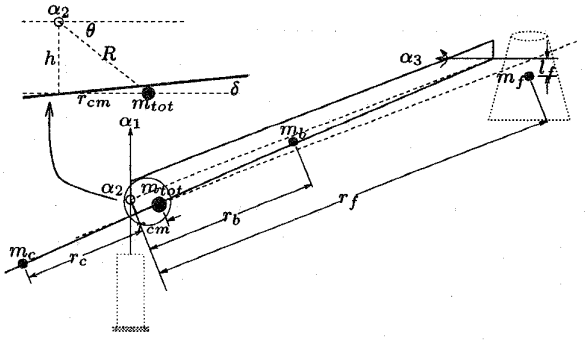

Figure 4: Simplied picture of the overall experimental setup The arrows associated with α_1 and α_3 represent the axes of rotation. α_2 axis is coming out of the page, as indicated by the empty circle.

m_b	2.872	kg	r_b	30	cm
m_c	6.427	kg	r_f	143.5	cm
m_f	2.215	kg	r_{flap}	26	cm
I_{xx_b}	0.7537	kg-m^2	l_f	2.129	cm
I_{zz_b}	1.731	kg-m^2	h	4.143	cm
I_{yy_f}	0.0475	kg-m^2	τ	0.3	sec

Table 1: Table of experimentally determined physical constants

m_i	mass of each object
r_i	distance of center of mass of each object from the α_2 axis
I_{yy_f}	moment of inertia of the fan about α_3 axis
I_{zz_b}, I_{xx_b}	moment of inertia of the base about α_1 and α_2 axis at $\alpha_2 = 0$
l_f	distance of center of mass of the fan from the α_3 axis
r_{flap}	moment arm of $F_\perp$
h	distance from the α_2 axis to the plane on which m_is lie
$F_\parallel, F_\perp$	components of the vectored force parallel and normal to the motor axis.

Values for these physical parameters are gathered in Table 3.1. The total mass of the system is

$$m_{tot} = m_f + m_b + m_c.$$

The location of the center of the mass of the whole system is

$$r_{cm} = \frac{r_f m_f + r_b m_b + r_c m_c}{m_{tot}}.$$

The total moment of inertia of the system around α_1 and α_2 axes are

$$I_{zz} = I_{zz_b} + m_c r_c^2 + m_f r_f^2$$

and

$$I_{xx} = I_{xx_b} + m_c r_c^2 + m_f r_f^2,$$

respectively. Since $\delta \sim 0$, the effective distance of m_{tot} from α_2 axis is

$$R \approx \sqrt{h^2 + r_{cm}^2}$$

and it also follows that

$$\tan\theta \approx \frac{h}{r_{cm}}.$$

Note that $\theta = \frac{\pi}{2}$ when $r_{cm} = 0$, meaning that the base is "balanced," and $\theta \to 0$ as $r_{cm} \to \infty$.

Now, consider the potential and the kinetic energy term of the system:

$$V = g\big(m_{tot}R(1 + \sin(\alpha_2 - \theta)) + m_f l_f (1 - c_3)\big) \quad (1)$$

$$T = \frac{1}{2}\big(I_{zz}c_2^2\dot{\alpha}_1^2 + I_{xx}\dot{\alpha}_2^2 + I_{yy_f}\dot{\alpha}_3^2 + 2\gamma c_2(c_3\dot{\alpha}_1 + s_3\dot{\alpha}_2)\dot{\alpha}_3\big) \quad (2)$$

where $\gamma = m_f l_f r_f$ and c_i and s_i are short hand notations for $\cos\alpha_i$ and $\sin\alpha_i$. After a detailed calculation using Lagrange's equations, the equations of motion for the system can be written as

$$M(\alpha)\ddot{\alpha} + C(\alpha,\dot{\alpha})\dot{\alpha} + N(\alpha) = T(\alpha, F), \quad (3)$$

where

$$M(\alpha) = \begin{bmatrix} I_{zz}c_2^2 & 0 & \gamma c_2 c_3 \\ 0 & I_{xx} & \gamma c_2 s_3 \\ \gamma c_2 c_3 & \gamma c_2 s_3 & I_{yy_f} \end{bmatrix}$$

$$N(\alpha) = \begin{bmatrix} 0 \\ m_{tot}Rg\cos(\alpha_2 - \theta) \\ m_f l_f g \sin\alpha_3 \end{bmatrix}$$

$$T(\alpha, F) = \begin{bmatrix} r_f c_2(F_\parallel s_3 - F_\perp c_3) \\ r_f c_2(F_\parallel c_3 + F_\perp s_3) \\ r_{flap}F_\perp \end{bmatrix}$$

and

$$C(\alpha,\dot{\alpha}) = -I_{zz}c_2 s_2 \begin{bmatrix} \dot{\alpha}_2 & \dot{\alpha}_1 & 0 \\ -\dot{\alpha}_1 & 0 & 0 \\ 0 & 0 & 0 \end{bmatrix} - \frac{\gamma}{2}\begin{bmatrix} 0 & \dot{\alpha}_3 c_3 s_2 & \dot{\alpha}_2 c_3 s_2 + 2\dot{\alpha}_3 c_2 s_3 \\ -\dot{\alpha}_3 c_3 s_2 & 0 & -2\dot{\alpha}_3 c_2 c_3 - \dot{\alpha}_1 c_3 s_2 \\ \dot{\alpha}_2 c_3 s_2 & \dot{\alpha}_1 c_3 s_2 + 2\dot{\alpha}_2 s_2 s_3 & 0 \end{bmatrix}.$$

$M(\alpha)$ is the generalized inertia matrix, $C(\alpha,\dot{\alpha})$ is the Coriolis matrix, $N(\alpha)$ is the matrix of gravity terms and $T(\alpha, F)$ is the matrix of applied joint torques. Although an even more sophisticated equation of motion can be obtained by keeping the Coulombic damping term and taking aerodynamic effects into consideration, the above model is sufficient as a starting point.

The model does not include the gyroscopic terms that result from the angular momentum of the whirling fan blade. However, since the four bar mechanism constrains the fan to rotate about an axis that is always parallel to the ground, the gyroscopic forces generated by rotation of the fan blade couple with pitch motion are completely taken up by the stand and hence do not enter into the dynamics. Additional gyroscopic forces are present due to rotation about α_1 coupled with the fan blade rotation. These effects are negligible for $\dot{\alpha}_1 \ll 1$ and hence we ignore them here.

3.2. Static fan force identification. A reliable correspondence between the input PWM pulse widths into the speed controller and two R/C servos and the output force of the ducted fan was established experimentally. The complex shape of the ducted fan made it difficult to determine a closed form formula for the relationship between inputs to the fan—the motor speed and two flap angles—and the output vectored force. Instead, the fan was mounted on a sensitive six-DOF force-torque sensor with a low pass filter to cut off the motor vibration to

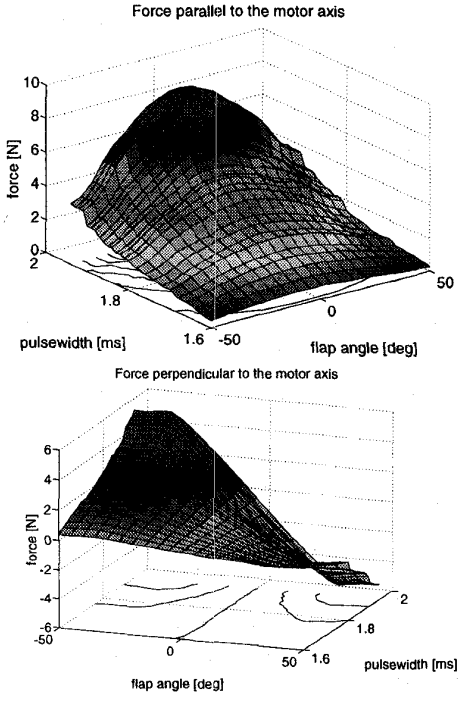

Figure 5: 3D contour and surface plots of the vectored force

the sensor, and run in an open-loop at a constant motor speed and flap angles. A simple analysis of the force-torque sensor data gave the fan force for that particular motor speed and flap angles combination. Figure 5 shows the graph generated from the experimental data.

3.3. Model validation. The equations of motions and the physical parameters were confirmed by comparing the results of the actual run and computer simulation. A PID altitude controller that regulated the α_2 angle with the other two angles held fixed at zero configuration was implemented on the actual system, and the data (joint angles and velocities and control efforts) from the run was compared against that of simulation on Matlab using an identical controller, as shown in Figure 6.

Initially, no time delay was assumed, but a large discrepancy in response could not be accounted for by anything else than a relatively large time delay in the motor response. This time delay is caused mainly by the slew rated response characteristic of the speed controller, which is used control the motor speed. This safety feature may be necessary for human controlled model airplanes, but is an undesirable feature for an automatically controlled system such as this. After several somewhat arbitrary guesses, $\tau = 0.3$ was chosen, and the matching between actual run and simulation became acceptable. The following figure also shows a somewhat poor matching when no time delay is assumed on the R/C servo response.

4. Initial control experiments

Altitude control using a PID controller was the ideal starting point because it is extermely simple to implement

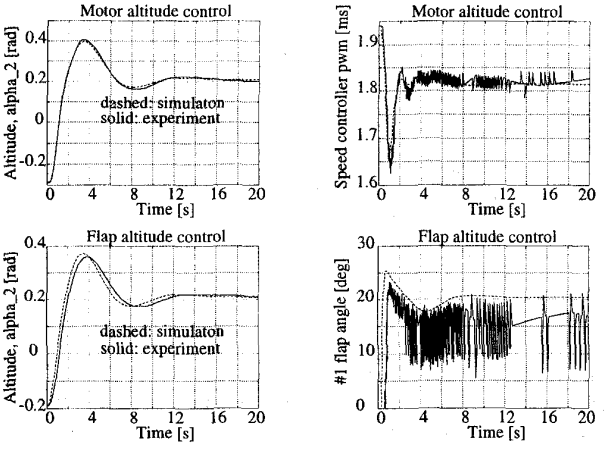

Figure 6: Comparison of altitude and control effort of the actual and the simulated data

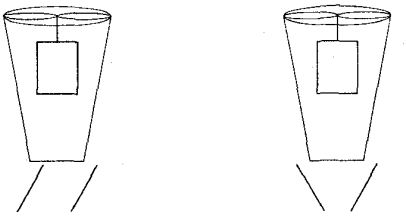

Symmetric flap setting Anti-symmetric flap setting

Figure 7: Two different flap settings. In both cases, the flaps are ganged. In anti-symmetric setting, the end can be closed off and apply a backward thrust at the flap angle of about 40°. In symmetric setting, the fan can output a sideways force as well as a downward force.

and has already been tried to some extent while validating the model. There were two different settings for the altitude control: flap control and the motor speed control. Although two flaps can move independently, the dynamics of the fan and the system in general have not been studied enough to warrant control algorithms that can make use of independently moving flaps. Hence, the flaps are ganged in either symmetric or anti-symmetric settings, as shown in Figure 7. Figures 8 and 9 are typical behavior of the two controllers for step inputs.

In general, the flap control performed better; it converged to the goal position slightly faster than when the motor control was used. This is due to the large time delay of the speed controller, which controls the motor speed. Using the classical linear control theory, the requirements for stability were determined and performance was predicted for an arbitrarily picked gain schedule, and then confirmed in actual runs. Since the PID controller was merely a tool for model validation, no effort to optimize for robust performance was made.

One of the largest limitations on performance is the actuator saturation, which can be viewed as an additional non-linearity of the system, occurs when a large altitude change is commanded, as shown in Figure 10. An onset of integrator windup problem can be seen from the figure as well. For these reasons, identification of the actuator dynamics is crucial for agressive controller design.

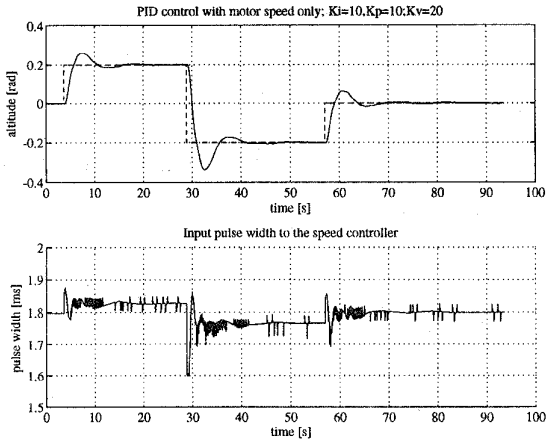

Figure 8: Set point tracking using motor control

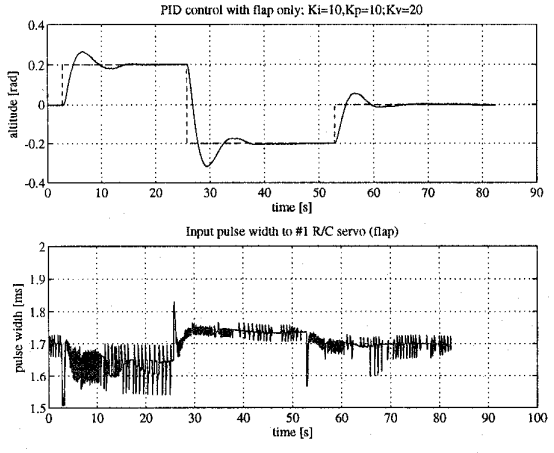

Figure 9: Set point tracking using flap control

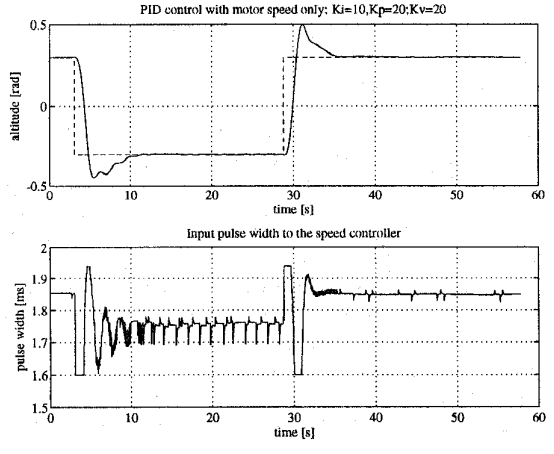

Figure 10: Example of actuator saturation for motor control. Upper and lower saturation points are 1.94ms and 1.60ms for motor speed control.

5. Conclusions and Future Work

The vectored thrust engine which we have described here provides a challenging platform for nonlinear robust control theory. In addition to nonlinearities which are present due to the mechanical nature of the system, there are also nonlinearities present due to the aerodynamics of the control surfaces and saturation of the fan motor. The system contains a large uncertainty since detailed modelling of the flow of air through the unit is not easily obtained in a form useful for control. High-performance control of this system will push the developement of new tools which can simultaneously incorporate the nonlinear and uncertain nature of the system.

A loopshape controller that controls both the pitch angle and the altitude was implemented. This MIMO controller uses feed-forward of the α_2 and α_3 positions to cancel out the static nonlinearies of the plant, such as the restoring force due to gravity. Initial experiments in this direction show that this is superior to controllers using simple feedback on the joint angles, and is well within the capabilities of the hardware and software currently available. However, more detailed models of the aerodynamic properties of the system are required in order to fully exploit the system's behavior.

One additional nonlinear effect which is present in the system which has not been mentioned previously is the behavior of the system near the ground. When the fan unit operates very close to the ground, the thrust generated by the fan varies significantly from operation far away from the ground. This occurs because the air bounces off of the ground and generates non-uniform flow patterns in the region near the flaps. Preliminary experiments indicate that the thrust characteristics depend strongly on the distance of the fan from the ground and also the angle that the fan makes with the ground. We are currently exploring the consequence of this effect on the overall control of the system.

Our eventual goal is to use this system to test linear and nonlinear control strategies. One example scenario is to design a controller which starts with the system at hover, transitions to forward flight and flies two complete orbits, then reverse direction and flies back for a single orbit. The performance of the controller would be measured by the amount of time required to complete this manuever. The nonlinear nature of the system, including the reverse thrust capabilities of the fan, make this an extremely challenging problem with applications to other high-performance control systems.

Acknowledgements. We would like to thank Matt Tucker, who built the PWM controller board, and Mateo Vasquez, who built the stand. We also received advice, assistance, and encouragement from Bob M'Closkey, Sudipto Sur, and John Doyle.

References

[1] B. Gal-Or. *Vectored Propulsion, Supermaneuverability and Robot Aircraft.* Springer-Verlag, 1990.

[2] D. Kuchemann and J. Weber. *Aerodynamics of Propulsion.* McGraw Hill, 1953.

[3] B. W. McCormick. *Aerodynamics of V/STOL Flight.* Academic Press, 1967.

[4] R. M. Murray and E. L. Wemhoff. *Sparrow 2.0 Reference Manual.* California Institute of Technology, 1994.